Design and Manufacturing of an Outer-Rotor BLDC Motor with Integrated Sensorless Drive for Automotive Cooling Fan Applications

Fazel Pourmirzaei Deylami, Mahdi Akbari, Maedeh Emami, Mohammad Amin Rezaei Gazik, Ali Ashrafian, and Mohammad Javad Kamali

Abstract—**This article proposes a 13.5-volt, 450-watt outer-rotor brushless DC (BLDC) motor for automotive radiator cooling fan applications. The design and modeling of the proposed BLDC motor are presented in some detail. Dynamic-transient analysis of the proposed motor is performed through finite element method (FEM) simulations using the ANSYS MAXWELL software. An integrated sensorless drive system is designed for the proposed motor which uses the phase voltage zero-crossing to detect the rotor position using the virtual neutral point scheme. The motor drive system simulation is performed through the MULTISIM software and the system's performance is evaluated. Thermal analysis of the drive system is essential due to the strict automotive considerations. In this regard, the thermal analysis of the integrated drive system is performed through the 3D FEM simulations using the SIEMENS FLOTHERM software. In order to validate the simulations, a prototype of the proposed motor in compliance with all automotive considerations is manufactured and some experimental tests including the functional and wind-tunnel tests are applied to evaluate the design accuracy. The results show that the proposed motor can be a good option for automotive fan applications.**

Index Terms—**Automotive cooling fan, BLDC motors, Finite element analysis (FEA), Integrated drive, Outer-rotor, Sensorless drive, Thermal analysis**

I. INTRODUCTION

DIRECT current (DC) electrical machines are widely used in the automotive industry as electromechanical subsystems. DC motors in the power range of up to 800 watts have been used in various parts of the vehicle, such as the window lifter motor [1], electric power steering (EPS) [2], the fuel pump [3] and water pump motor [4], the wiper motor [5], the radiator cooling fan motor [6] and so on. Due to the advancement of automotive industry technologies, many other sub-systems in motor vehicles are also moving towards electrification. For example, sub-systems such as water pump and steering system, which used to be completely mechanical systems, have moved towards electrification in recent years, and today the use of electric water pump systems and electric steering systems is very common and these electrified systems are widely used in the automotive industry.

Most of the automotive electric motors since the past are permanent magnet DC motors (PMDC) [7]. The use of these motors is associated with the mechanical commutation system (Commentator and brushes). High mechanical losses and sparks in the mechanical commutation system reduce the efficiency, increase the acoustic noise and reduce the durability of the machine [8]. In recent years and with the development of the electric machine industry, the use of brushless DC motors (BLDC) as a safe alternative to PMDC motors has become very popular. BLDC machines can significantly increase the efficiency due to the elimination of the mechanical commutation system using the electrical drive system. In addition, the acoustic noise in these machines is less and their durability is longer than PMDC motors [9].

One of the most important automotive applications of DC motors is to use them as a radiator cooling fan motor [6, 7, 10]. These motors are designed in the power range of 80 to 800 watts and the operational speed range of 2500 to 3500 rpm. Speed control in PMDC fan motor is mainly accomplished in two ways. The first method is the double-speed control system (relay-resistor system). In this method, the motor can only operates in high or low speed modes. At high speed mode, the motor terminal is directly connected to the power supply (13.5 volts) and at low speed mode, a resistor is placed in series between the motor terminal and the power supply, and as a result, a lower voltage is sent to the motor terminal, which causes the motor speed to decrease. Using this method, in addition to high losses in the resistor, it is not possible to continuously control the motor speed. The second method is to use a DC chopper to control the motor input voltage [11, 12].

Using this method can eliminate the wasted power in the speed reducing resistor and provide the possibility of continuous speed control. However, the use of BLDC motors can provide the possibility of continuous speed control along with the elimination of the mechanical commutation system, which leads to a significant increase in motor efficiency.

The design of BLDC motors is largely similar to permanent magnet synchronous machines (PMSMs), except that the back electro motive fore (BEMF) characteristic is sinusoidal in PMSM machines and trapezoidal in BLDC machines. Therefore, the design methods of these machines are very close to each other. Analytical methods for the design of brushless machines are presented in references [13, 14]. Numerical optimization methods with the aim of achieving the highest efficiency and limiting the torque ripple are among the topics that are considered in the field of optimal design of brushless motors. In these studies, the dimensional and geometrical parameters of the motor are selected in such a way that the motor has the highest efficiency and the lowest ripple torque. For example, in references [15, 16], the effects of choosing the number of poles and teeth as well as the effects of the shape of the slots on the operating parameters of the motor have been evaluated.

BLDC drive structures and methods are very diverse. In general, 6-switch drive structures are the most common BLDC machine drive methods, which are discussed in references [17] and [18], respectively. Estimation of the rotor position is critical to determine the switching times. In order to determine the position of the rotor, Hall Effect sensors can be used in the stator [19]. In addition, there are several sensorless drive and control methods for BLDC machines. These methods are usually used to determine the position of the rotor based on the internal characteristics of the machine, such as the BEMF characteristic [20], the flux linkage characteristic [21], the inductance characteristic [22], etc. Start-up process of BLDC motors is another challenge to be considered. Soft start of the motor should be accomplished by determining the initial position of the rotor and then gradually increasing the voltage and frequency. In reference [23], the i-f method is used to start the BLDC motor, and in reference [24], a starting method is presented to avoid the reverse rotation of the rotor.

In this paper, a 450 W outer-rotor BLDC motor equipped with a modular sensorless drive system is proposed for radiator cooling fan application. In this 8-pole motor, the zero-crossing of the stator phase voltage is used to determine the position of the rotor and create a switching signal to continuously control the speed of the motor. According to the automotive application of the motor, the use of the simplest and least expensive methods, materials and equipment is considered for manufacturing of the proposed prototype.

II. BLDC MOTOR STRUCTURE

Figure 1 shows the proposed BLDC motor structure. The proposed outer-rotor BLDC motor has 8 surface-mounted permanent magnet poles located on the inner surface of the rotor. The stator core has 12 teeth/slots, where the concentrated three-phase winding with delta connection is placed inside the slots. After winding the stator core, the stator is placed inside the rotor space and connected to the drive terminals through the terminals located behind it. The board designed for the drive is placed inside the heat sink housing and the heat sink is connected to the stator through three screws. As shown in Figure 1, the proposed motor/drive system has a modular and integrated structure that easily enables connecting and disconnecting the drive and motor from each other. Figure 2 shows the complete automotive radiator cooling fan module (CFM). As shown in this figure, the fan module has 7 blades with a diameter of 370 mm. Detailed dimensional and operational parameters of the BLDC motor and fan module are presented in Table I.
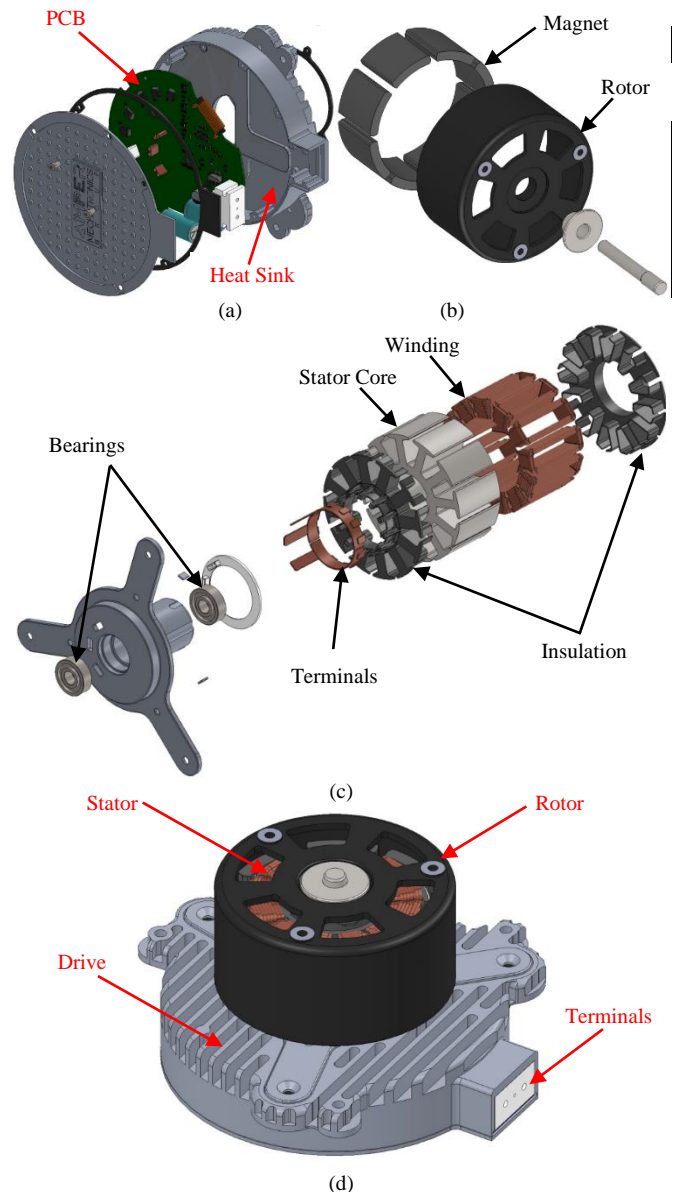
Fig.1. Structure of the proposed BLDC motor. (a) Drive system, (b) Rotor, (c) Stator, (d) Assembled motor.
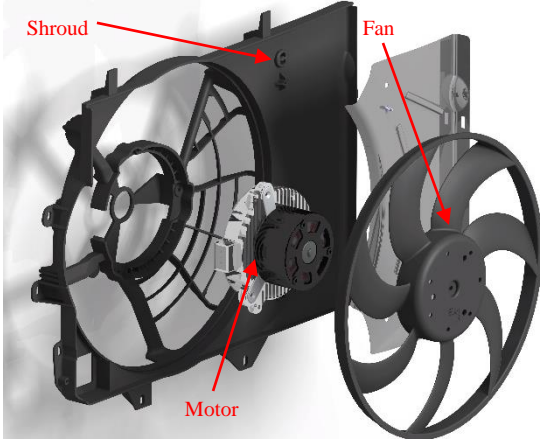
Fig.2. Automotive radiator cooling fan module (CFM).

TABLE I
OPERATIONAL AND DIMENSIONAL PARAMETERS OF THE CFM

Operational Quantities	Symbol	Value
Rated Voltage (DC)	V_{dc}	13.5 V
Rated Current	I_{dc}	33.33 A
Rated Power	P_{in}	450 W
No Load Speed	n_{nl}	4200 rpm
Full load Speed	n_{fl}	3000 rpm
Nominal Torque	T_e	1.2 Nm
Operating Temperature	T_{op}	110 °C
Fan Quantities	**Symbol**	**Value**
Number of Blades	N_b	7
Outer Diameter	D_{of}	370 mm
Hub Diameter	D_{hf}	136 mm
Shroud Length	L_{sh}	580 mm
Shroud width	W_{sh}	420 mm

TABLE II
PREDETERMINED PARAMETERS OF THE BLDC MOTOR

Quantity	Symbol	Value
Air Gap Length	g	1 mm
Average Flux Density	B_{av}	0.3 T
Magnet Residual Flux Density	B_r	0.41 T
Teeth Flux Density	B_t	1.8 T
Stator/Rotor Flux Density	B_{ys}/B_{yr}	1.6 T
Electric Loading	A	10000 At/m
Aspect Ratio	K_{dim}	0.6
Shape Factor	K_s	1.4
Winding Factor	K_w	0.866
Reluctance Factor	K_r	1.1
Leakage Factor	K_l	0.9
Fill Factor	K_{fill}	0.3
Magnet Covering Factor	G_m	0.95
Current Density	J	6 A/mm²
Number of phases	m	3
Number of Poles	P	8
Number of Slots/Teeth	s/t	12
Number of Magnets	N_{mag}	8
Number of Slot/Pole/Phase	q	0.5

III. MOTOR DESIGN PROCESS

In this section, the design process of a radial-flux outer-rotor brushless DC motor is described in some detail. This machine is a 450 Watt, 13.5 Volt, and 3000 rpm motor with a nominal torque of 1.2 Nm. The design algorithm is based on the well-known methods of designing permanent magnet synchronous machines (PMSMs) [25, 26]. The predetermined values in the proposed BLDC motor design are given in Table II.

A. Main Dimensions

The main dimensions of the machine include parameters such as outer diameter, axial length, air gap length, pole pitch, and slot pitch, which are determined at the beginning of the design through the power equation [25, 26]. The outer diameter of the motor can be calculated as follows:

$$D = \left(\frac{P \times P_o}{K_{\dim} \times C \times n_{rps} \times \pi} \right)^{\frac{1}{3}} \tag{1}$$

Where, P_o is the rated output power, n_{rps} is the rated speed (revolution per second), and other parameters can be obtained as follows:

$$\begin{cases} K_{\dim} = \dfrac{L}{\tau_p} \\ C = K_s K_w B_{av} A \pi^2 \end{cases} \tag{2}$$

Where, L is the axial length and τ_p is the pole pitch. The stator slot pitch and rotor pole pitch can be defined as Equation (3) and the axial length of the proposed motor can be obtained from Equation (4):

$$\begin{cases} \tau_p = \dfrac{\pi D}{P} \\ \tau_s = \dfrac{\pi D}{s} \end{cases} \tag{3}$$

$$L = \frac{P_o}{C \times n_{rps} \times D^2} \tag{4}$$

B. Stator and Rotor Design

In order to calculate the dimensions of stator and rotor components, it is necessary to first calculate the flux passing through different parts of the motor. The total flux of the motor, the magnetic flux per pole and the magnetic flux per tooth can be calculated as follows:

$$\begin{cases} \varphi_{tot} = B_{av} \times \pi \times D \times L \\ \varphi_P = \dfrac{\varphi_{tot}}{P} \\ \varphi_t = \dfrac{\varphi_{tot}}{t} \end{cases} \tag{5}$$

After calculating the magnetic flux in the stator and rotor, the thickness of the permanent magnet can be obtained from following equation [25, 26]:

$$h_m = \frac{B_{av} \times \mu_r \times G_m \times K_r \times K_l \times g}{G_m \times K_l \times B_r - B_{av}} \tag{6}$$

By assuming the appropriate maximum allowable flux in the teeth, rotor yoke, and stator yoke, the teeth width and the thickness of the stator and rotor yoke can be obtained as follows:

$$\begin{cases} w_t = \dfrac{\varphi_t}{B_t \times L} \\ w_{ys} = \dfrac{0.5 \times \varphi_P}{B_{ys} \times L} \\ w_{yr} = \dfrac{0.5 \times \varphi_P}{B_{yr} \times L} \end{cases} \tag{7}$$

In order to obtain the length of the stator teeth, it is first necessary to design the stator winding and determine the area required for the placement of the winding. The number of turns of the stator winding can be calculated from the equation of the induced voltage in the winding [25, 26]. The number of turns per phase, and the number of turns per coil, can be calculated as follows:

$$\begin{cases} N_{ph} = \dfrac{0.5 \times V_{dc}}{K_s \times K_w \times \varphi_{tot} \times 2 \times n_{rps}} \\ N_{coil} = \dfrac{N_{ph} \times m \times P}{s} \end{cases} \tag{8}$$

After calculating the winding turns, the cross section of the wire and the minimum slot area required for the windings can be obtained as follows:

$$\begin{cases} A_{wire} = \dfrac{I_{coil}}{J} \\ A_{slot} = \dfrac{N_{coil} \times A_{wire}}{K_{fill}} \end{cases} \tag{9}$$

The last dimensional parameter of the stator core is the length of the stator slots. According to the trapezoidal shape of the slots, the length of the slots can be calculated as follows, where b_{s1} and b_{s2} are the top and bottom width of the slot [25, 26]:

$$h_s = \frac{4A_{slot}}{b_{s1} + b_{s2}} \tag{10}$$

Using the above-mentioned equations, the dimensional parameters along with the material grades of different parts of the designed machine are presented in Table III.

TABLE III
DESIGN VALUES OF THE PROPOSED MOTOR

Quantity	Symbol	Value
Outer Diameter	D_o	100 mm
Axial Length	L	30 mm
Tooth Width	w_t	4.5 mm
Slot length	h_s	17 mm
Stator/Rotor Yoke Width	w_{ys}/ w_{yr}	3.8 mm
Magnet Thickness	h_m	6 mm
Number of Turns/Coils	N_{coil}	17
Number of Parallel Branches	N_p	2
Winding Connection	Δ (Delta)	-
Part	**Material**	**Grade**
Stator Core	Steel	M700-50A
Rotor Yoke	Steel	ST37
Magnet	Ferrite	Y35
Winding	Copper	1.25mm/180°C

IV. DRIVE SYSTEM STRUCTURE

Figure 3 shows the structure of the proposed BLDC drive system. This system consists of a 6-switch three-phase inverter that supplies three-phase trapezoidal voltage to the motor terminals. Estimation of rotor position is necessary to determine switching sequences. This can be performed by placing Hall Effect sensors in the stator or by using sensorless methods. In this study, sensorless control of the motor is accomplished using zero crossing of the stator phase voltage. For this purpose, a virtual neutral point is created through three resistors and a low-pass filter is applied to the phase voltage in order to remove high frequency components and achieve a smooth waveform. The generated signal is sent to the microcontroller for processing and creating switching sequences. Motor speed control is performed through controlling the voltage level of the motor terminals. This can be applied by changing the duty cycle of a 25 kHz PWM signal created by the microcontroller. In order to reduce voltage and current ripple and manage electromagnetic interference (EMI), an LC low-pass filter is installed at the input terminals of the inverter. In addition, some sub-circuits are included in drive system for overcurrent and reverse voltage protection. Figure 4 shows the different parts of the designed drive system. The specifications of the components used in the drive system are presented in Table IV.
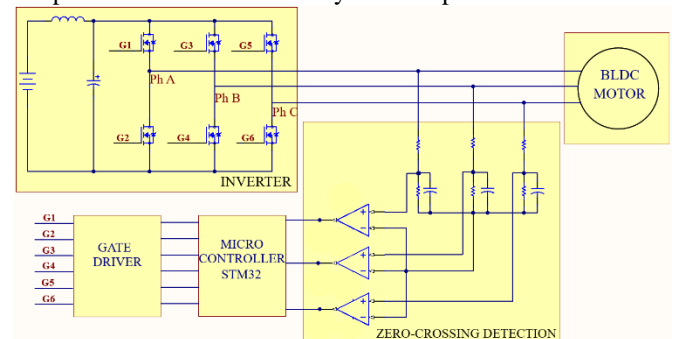

Fig. 3. Structure of the BLDC drive system.
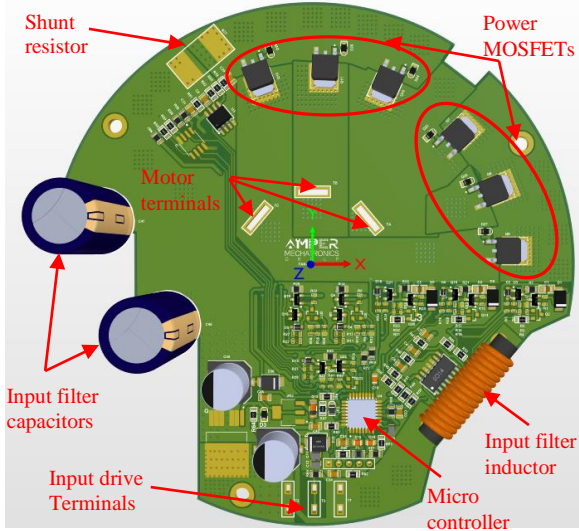
Fig. 4. Designed BLDC Sensorless Drive system.

TABLE IV
SPECIFICATIONS OF THE DRIVE SYSTEM

Quantity	Symbol	Value
Rated Input Voltage	V_{dc}	*13.5 V*
Operating Voltage	-	*6-18 V*
Rated Input Power	P_{in}	*450 W*
Switching Frequency	f_s	*25 kHz*
Communication Signal	-	*100 Hz PWM*
Input LPF Inductor	L_{in}	*4.5 µH*
Input LPF Capacitor	C_{in}	*2×2200 µF*
Power MOSFETs	-	*6×IRLR7843*
Microcontroller	-	*STM32F030A6T6*
VZC Circuit VNP Resistor	R_n	*3×10 kΩ*
VZC Circuit LPF Resistor	R_{fn}	*3×2.2 kΩ*
VZC Circuit LPF Capacitor	C_{fn}	*3×300 nF*

V. PROTOTYPE MANUFACTURING

In order to confirm the simulation results of the designed motor and drive, a prototype of the proposed system is manufactured. Prototype manufacturing of the BLDC motor-drive system can be divided into two separate processes. The first is the manufacturing of motor parts, and the other is the manufacturing and assembly of the printed circuit board (PCB) of the drive system. Motor parts include stator core laminations, shaft, bearings, stator winding, winding insulators, stator terminals, rotor housing and permanent magnets. The drive system consists of a PCB board placed inside the heat sink housing. The integrated and modular design of the system allows easy installation and separation of the drive from the motor. Figure 5 shows the manufactured prototype along with the different parts of the motor and drive.

VI. DISCUSSION AND RESULTS

In this section, the accuracy of the designed BLDC motor-drive system is evaluated through detailed electromagnetic and thermal finite element (FE) simulations. In addition, the results of some experimental tests on the manufactured prototype are

presented in this section to validate the accuracy of the simulation results.

A. Electromagnetic Analysis

The electromagnetic modeling and FEM simulation of the proposed BLDC motor is performed in this section to evaluate the performance of the motor. The results of the electromagnetic simulations are compared with the results of some fictional tests applied to the motor prototype. The FEM simulation is performed using ANSYS MAXWELL software using 2D model of the BLDC motor. Figure 6 shows the 2D model of the BLDC motor. As shown in this figure, due to the geometric symmetry, only 1/4 of the motor geometry is considered for modeling the 8-pole BLDC motor. This can significantly increase the speed of calculations in FE simulation.

Figure 7 shows the no-load and full-load distribution of the magnetic flux density in different parts of the motor. According to this figure, the maximum flux density occurs in the stator teeth. The maximum no load flux density obtained about 1.5 T and the maximum full load flux density reaches up to 1.7 T. Figure 8 shows the amplitude and the radial component of the flux density in the air gap. As shown in this figure, the average value of flux density in the air gap is about 0.31 T and the peak value reaches to about 0.49 T. In addition, the peak-to-peak variation of the radial component of the flux density is obtained about 0.9 T. Due to the FEM simulation results, the values obtained for the flux density distribution confirms the selected values for flux density at the beginning of design.
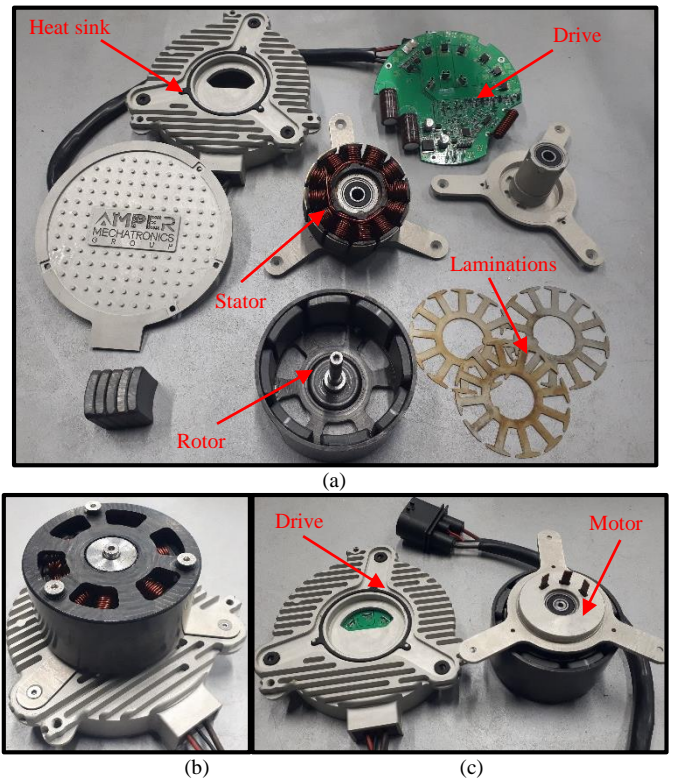

Fig. 5. Manufactured Prototype. (a) Different parts of the Prototype, (b) Assembled BLDC machine, (c) Motor and Drive.
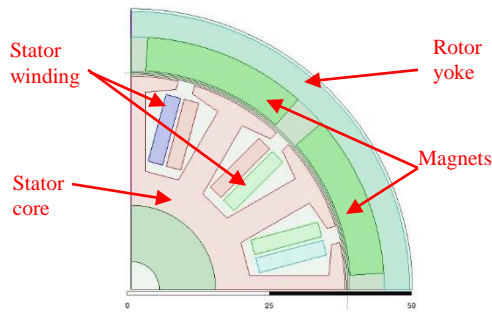
Fig. 6. 2D model of the proposed BLDC motor.

(a)   (b)
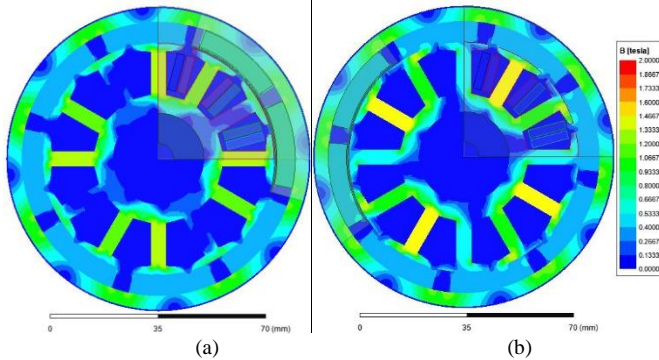
Fig. 7. Flux density distribution. (a) No load, (b) Full load.

(a)

(b)
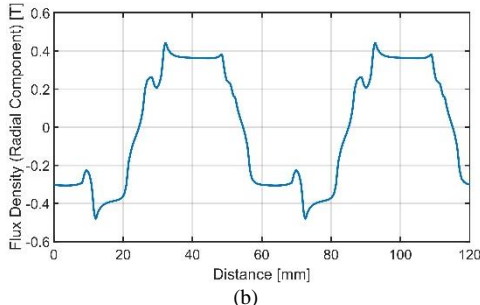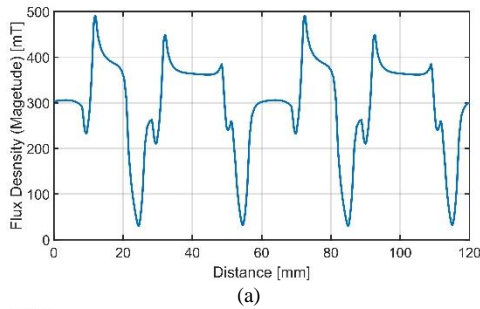
**Fig. 8.** Gap flux density. (a) Magnitude, (b) Radial component.

The operational characteristics of the proposed BLDC motor the obtained from FEM simulation are reported in this section. Figure 9 shows the no load characteristics of the motor at the speed of 3900 rpm. As shown in Figure 9(a), the no load voltage has a trapezoidal profile with a peak value of about 13 V. Figure 9(b) shows the ideal no load current is close to zero whithout consideration of the mechanical rotational losses. The no load torque of the proposed BLDC motor is presented in Figure 9(c). This figure shows that the peak-to-peak value of the no load torque is obtained about 0.26 Nm that can be mentioned as cogging torque. The cogging torque ripple percentage value is about 10.5 % of the rated torque value of the motor.

(a)

(b)

(c)
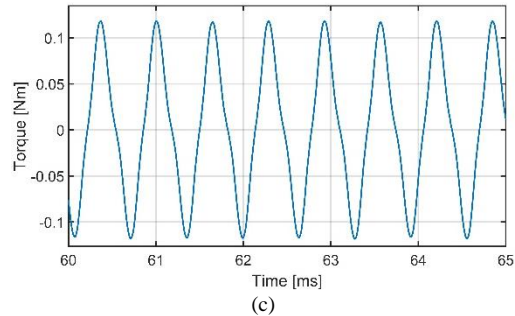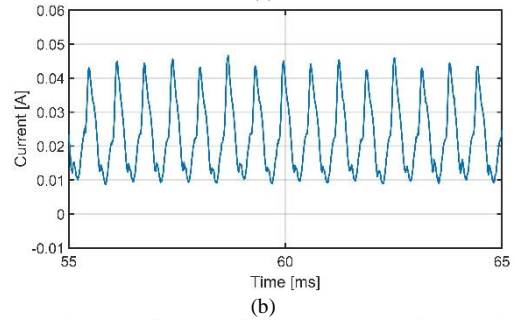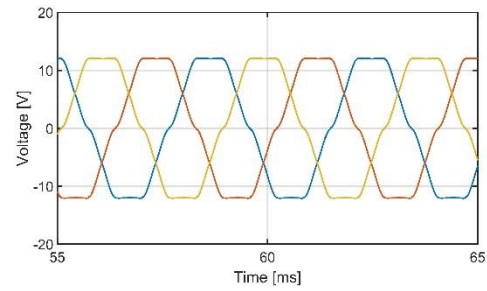
Fig. 9. No load characteristics. (a) Induced no load voltage, (b) no load current, (c) no load torque.

The full load characteristics of the motor are presented in Figure 10. The full load simulation is performed at the load torque of 1.2 Nm and the ideal acceleration of the motor is reported in this section. The time required to reach the steady state under the above mentioned load application process is about 150 ms. Figure 10(a) shows the torque profile of the proposed BLDC motor during the acceleration process. The peak torque reaches to more than 7 Nm and the average torque in steady state abviously reaches to 1.2 Nm and equals to the applied load torque. The peak-to-peak torque ripple is abtained about 0.4 Nm and the torque ripple obtained about 16.6 % of the average torque. The full load power supply current profile is shown in Figure 10(b). The peak current of the power supply during the ideal acceleration can reach to about 800 A and the average current reaches to about 34 A. The current ripple is obtained about 44 %. The ripple of the input current. Figure 10(c), and 10(d) show the line and phase current profiles of the delta connected three-phase winding of the BLDC motor, respectively. Due to these figures, the peak line current in steady state reaches to more than 50 A and this value is $3^{1/2}$ times of the phase current. The speed profile of the BLDC motor is shown in Figure 10(e). As can be seen in this figure, the rated speed of the motor reaches to about 3000 rpm at the rated mechanical load. In addition, it can be seen that the speed profile is very smooth and the speed deviations around the average speed value is very low.
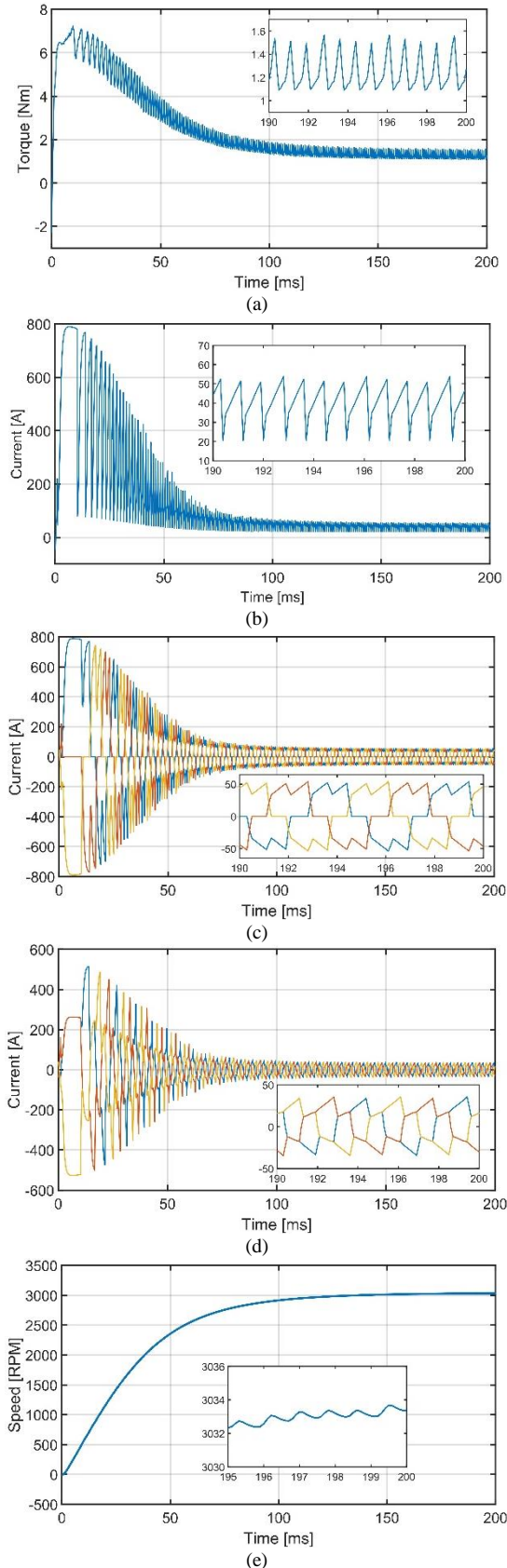
Fig. 10. Full load characteristics. (a) Torque, (b) Input currrent, (c) Line currents, (d) Phase currents, (e) Speed profile.

Figure 11 shows the main output characteristics of the proposed BLDC motor. Figure 11(a) and Figure 11(b) show the torque-speed and current-speed characteristics, respectively. The constant torque/current area of the motor is specified in a speed range of zero to 3000 rpm and the constant power area is specified in a speed ragne of 3000 to 3900 rpm. According to the mentioned values, the speed regulation of the proposed motor can be obtained about 30 %. Figure 11(c) shows the torque-current characteristic of the motor. According to this figure the torque-current profile has an almost linear profile with a slop of about 35.29 mNm/A.

The experimental results of the functional tests applied to the manufactured prototype are presented in this section. Figure 12 shows the experimental setup of the BLDC motor. Figure 13 shows the no load and under load phase-to-phase voltage and current profiles of the proposed BLDC motor. The under load measurements performed when the load torque of 0.8 Nm is applied to the prototype at the speed of 3300 rpm. According to this Figure 13(c), the average input current under above mentioned loading condition is about 26 A and the aurrent ripple is about 11.5 %. Table V shows the camparison between the simulation results and the measurements at the under load condition. The results show that the simulations and measurements are in a good aggrement and the motor can operate at the expected working points due to the performed design process.
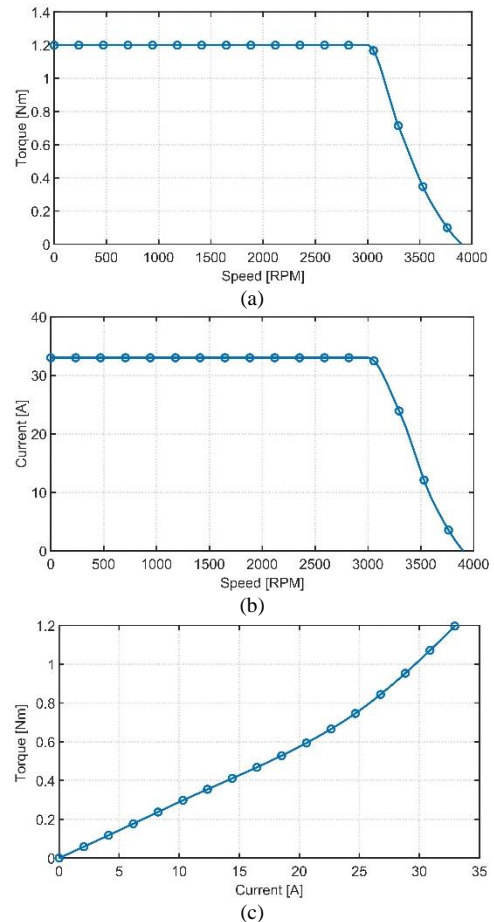
Fig. 11. Output characteristics. (a) Torque-speed, (b) Current-speed, (c) Torque-current profiles.
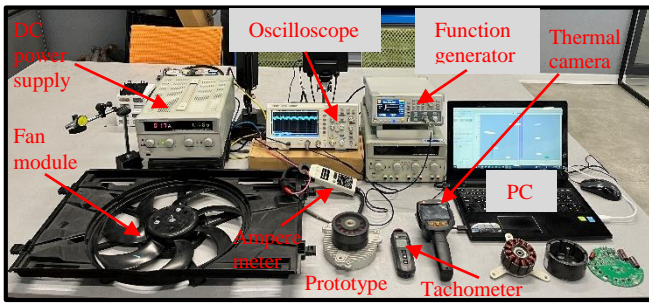
Fig. 12. Experimental setup.


(a)

(b)

(c)
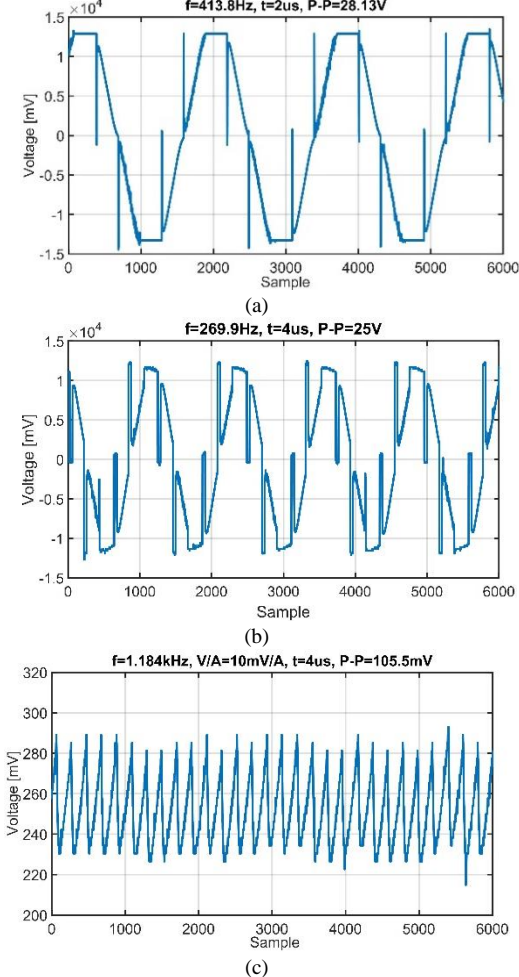
Fig. 13. Measured chatacteristivs. (a) No load voltage, (b) Under load voltage, (c) Under load current.

TABLE V
COMPARISON BETWEEN MEASUREMENT AND SIMULATIONS

Quantity	Simulation	Measurement
Voltage	13.5 V	13.5 V
Current	23.6 A	26 A
Speed	3300 rpm	3300 rpm
Torque	0.73 Nm	0.8 Nm
Efficiency	79 %	78.7 %

B. Thermal Analysis

In this section, the thermal analysis of the drive system is performed through finite element simulation using SIEMENS SIMCENTER FLOTHERM software and the results are compared with the experimental measurements using TESTO thermal imaging camera. This software is powerful enough to model multi-layer printed circuit board (PCB) details such as thermal vias and complex traces. In order to increase the accuracy of the thermal simulation, the entire drive system, including the covering package and heat sink, along with the BLDC motor, is placed in front of the air flow created by the fan module, and the temperature of the different parts of the drive system is obtained. In this simulation, the power consumption of power MOSFETs, input capacitors and inductor, reverse voltage protection (RVP) switch, voltage regulator and shunt resistor as the main sources of power loss is calculated in the worst condition and applied as simulation input in the software. The input parameters of thermal FEM simulation are presented in Table VI. Figure 14. Shows the simulation results and the thermal imaging results of the designed drive system. As shown in this figure, the maximum error of simulations is obtained about 5.4 % that shows the acceptable accuracy of simulations.


(a)

(b)

(c)

(d)
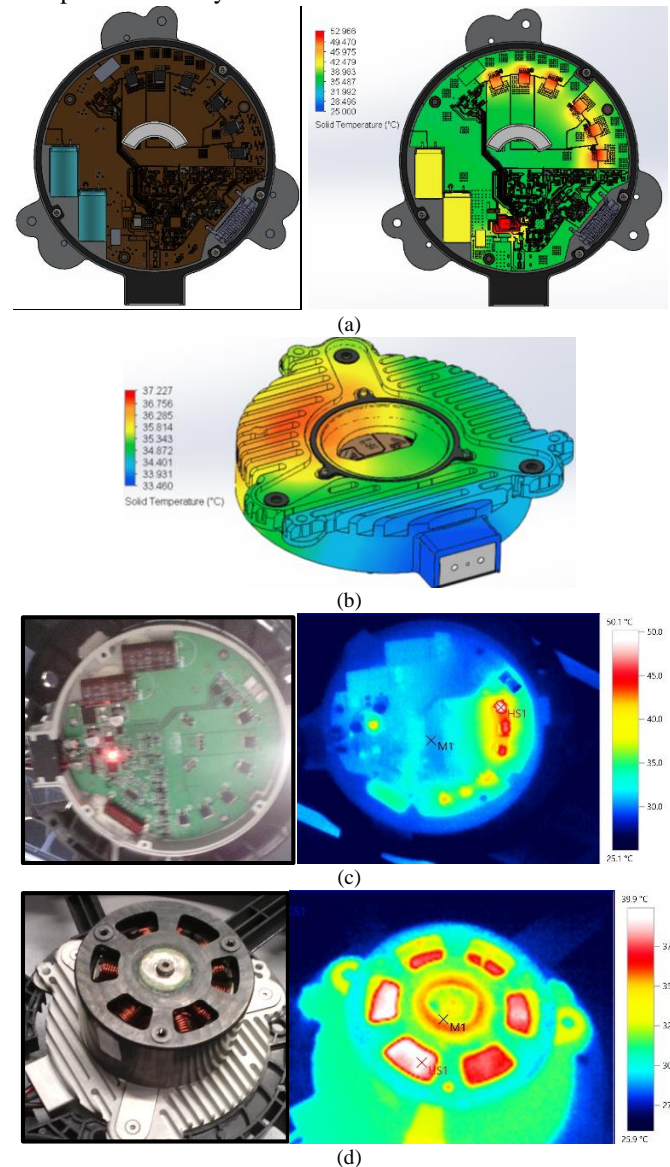
Fig. 14. Thermal evaluations. (a) PCB temperature distribution. (b) Heat sink, (c) PCB thermal measurement, (d) motor thermal measurement.

TABLE VI
INPUT PARAMETERS OF THE THERMAL SIMULATION (VOLTAGE: 13.5 V,
SWITCHING FREQUENCY: 25 KHZ, SWITCHING DUTY CYCLE: 0.67)

Quantity	Value
Input LPF Inductor Loss	*0.6 W*
Input LPF Capacitor Loss	*2×1.3 W*
RVP MOSFET Loss	*0.5 W*
Power MOSFETs Loss	*6×2.7 W*
Voltage Regulator Loss	*3.2 W*
Fan Flow Rate	*0.55 m³/s*
Ambient Temperature	*25 °C*
Ambient Pressure	*100 kPa*
Silicone Pad Conductivity	*2 W/m.K*
Silicone Cream Conductivity	*3 W/m.K*
Solder Conductivity	*78.4 W/m.K*
Plastic Package Conductivity	*5 W/m.K*

VII. CONCLUSION

This article proposes a 450 Watt, 3000 rpm, 1.2 Nm brushless DC motor with sensorless controller for automotive radiator cooling fan applications. The proposed structure is designed as an integrated and modular motor/drive system that can easily assembled. The electromagnetic design of the proposed outer rotor motor and the sensorless drive system are presented in detail. The sensorless control is performed through zero-crossing detection of the terminal voltage signal. Performance evaluation of the proposed BLDC motor is performed through finite element (FEM) simulations and the operational characteristics are reported. Thermal simulations of the drive system are performed through 3D finite element simulations to ensure that all the components operate in safe thermal conditions. In order to evaluate the design and simulation results, a prototype of the proposed motor/drive system is manufactured and some experimental measurements are done. The results show that the simulations and experimental results are in good agreement and the proposed modular system can be suitable for the automotive cooling fan applications.

REFERENCES

[1] A. Consoli, A. Bottiglieri, R. Letor, R. Ruggeri, A. Testa, S. De Caro, "Sensorless position control of DC actuators for automotive applications," *Conference Record of the 2004 IEEE Industry Applications Conference, 2004. 39th IAS Annual Meeting*, 03-07 October 2004.

[2] Y. K. Kim, S. H. Rhyu, I. S. Jung, "Reduction design of cogging torque of BLDC motor for EPS application," *14th Biennial IEEE Conference on Electromagnetic Field Computation*, vol. 14, pp. 978-986, 2010.

[3] T. W. Chun, Q. V. Tran, H. H. Lee, H. G. Kim, "Sensorless control of BLDC motor drive for an automotive fuel pump using a hysteresis comparator," *IEEE transactions on power electronics*, vol. 29, no. 3, pp. 1382-1391, May 2013.

[4] G. C. Lee, T. U. Jung, "Design comparisons of BLDC motors for electric water pump," *IEEE Vehicle Power and Propulsion Conference*, Oct. 2012.

[5] M. Sundaram, J. Chelladurai, M. Anand, M. S. Kumari, S. Sharma, M. E. Assad, "A Novel Approach to Energy-Optimized Variable-Speed Sensorless-Based Brushless DC Motors (BLDC) Control for Automotive Wiper Applications," *Arabian Journal for Science and Engineering*, May 2023.

[6] U. K. Potnuru, P. M. Rao, "An Innovative Methodology in Design of a Permanent Magnet Brushless DC Motor for a Particular Application," *International Journal on Emerging Technologies*, vol. 11, no. 2, pp. 468-474, 2020.

[7] M. Kane, S. Kulkarni, S. Antony, R. Kharat, N. Chaithanya, "Design and Control of a Light-Weight Drive-Integrated 48 V BLDC Motor for Radiator Fan in Hybrid Vehicle," *SAE Technical Paper*, 2015-01-1207, 2015.

[8] T. Kenjo, S. Nagamori, "Permanent-Magnet and Brushless DC motors," *Monographs in Electrical and Electronic Engineering 18, Oxford Science Publishing*, 1985.

[9] I. D. Chasiotis, Y. L. Karnavas, "A computer aided educational tool for design, modeling, and performance analysis of Brushless DC motor in post graduate degree courses," *Computer Applications in Engineering Education*, vol. 26, no. 4, Jul. 2018.

[10] A. J. Pawar, A. Patil, "Design and development of 48V PMBLDC motor for radiator fan application by using ANSYS Maxwell software," *IEEE 3rd International Conference on Sensing, Signal Processing and Security (ICSSS),* 2017.

[11] N. Shaharudin, M. Z. Hasan, S. M. Noor, "Direct Current (DC) Motor Speed and Direction Controller," *Journal of Physics: Conference Series, IOP Publishing*, vol. 2129, no. 1, p.p. 012035, Dec. 2021.

[12] M. Tuna, C. B. Fidan, S. Kocabey, S. Gorgulu, "Effective and reliable speed control of permanent magnet DC (PMDC) motor under variable loads," *Journal of Electrical Engineering and Technology*, vol. 10, no. 5, pp. 2170-2178, 2015.

[13] A. Kerem, "Design, implementation and speed estimation of three-phase 2 kW out-runner permanent magnet BLDC motor for ultralight electric vehicles," *Electrical Engineering*, vol. 103, pp. 2547–2559, 2021.

[14] T. Y. Lee, M. K. Seo, Y. J. Kim, S. Y. Jung, "Motor Design and Characteristics Comparison of Outer-Rotor-Type BLDC Motor and BLAC Motor Based on Numerical Analysis," *IEEE Transactions on Applied Superconductivity*, vol. 26, no. 4, June 2016.

[15] A. M. Ajamloo, A. Ghaheri, E. Afjei, "Multi-objective Optimization of an Outer Rotor BLDC Motor Based on Taguchi Method for Propulsion Applications," *10th International Power Electronics, Drive Systems and Technologies Conference (PEDSTC),* 12-14 Feb. 2019.

[16] S. T. Jo, H. S. Shin, Y. G. Lee, J. H. Lee, J. Y. Choi, "Optimal Design of a BLDC Motor Considering Three-Dimensional Structures Using the Response Surface Methodology," *Energies*, vol. 15, no. 2, Jan. 2022.

[17] O. D. R. Cárdenas, F. T. Romero, "Sensorless Speed Tracking of a Brushless DC Motor Using a Neural Network," *Mathematical and Computational Applications,* vol. 25, no. 3, Sep. 2020.

[18] S. M. Rad, M. R. Azizian, "Filterless and Sensorless Commutation Method for BLDC Motors," *Journal of Power Electronics*, vol. 18, no. 4, pp. 1086-1098, July 2018.

[19] X. Xu, X. Huang, Q. Hu, Z. Li, "An Improved Rotor Position Estimation Method for SPMSM with Misaligned Hall-Effect Sensor," *IEEE Transactions on Transportation Electrification*, May. 2023.

[20] Z. Zhang, "Sensorless back EMF based control of synchronous PM and reluctance motor Drives—A review," *IEEE Transactions on Power Electronics*, vol. 37, no.9, pp. 10290-10305, Mar. 2022.

[21] D. Chen, J. Wang, L. Zhou, "Adaptive Second-Order Active-Flux Observer for Sensorless Control of PMSMs with MRAS-Based VSI Non-linearity Compensation," *IEEE Journal of Emerging and Selected Topics in Power Electronics*, Mar. 2023.

[22] S. Ye, X. Yao, "A modified flux sliding-mode observer for the sensorless control of PMSMs with online stator resistance and inductance estimation," *IEEE Transactions on Power Electronics*, vol. 35, no. 8, pp. 8652-8662, Jan. 2020.

[23] A. Ungurean, V. Coroban-Schramel, I. Boldea, "Sensorless control of a BLDC PM motor based on I-f starting and Back-EMF zero-crossing detection," *12th International Conference on Optimization of Electrical and Electronic Equipment,* 2010.

[24] Y. C. Chang, Y. Y. Tzou, "A New Sensorless Starting Method for Brushless DC Motors without Reversing Rotation," *IEEE Power Electronics Specialists Conference*, 2007.

[25] J. Pyrhonen, T. Jokinen, V. Harbovcova, "Design of Rotating Electrical Machines," *John Wiley & Sons Ltd*., 2008.

[26] F. P. Deylami, A. Darabi, F, Asadi, A. Gharavi, "Design and Performance Evaluation of a Novel Axial-Flux Hybrid Motor with Permanent Magnet Rotor and Unpaired Damper Cage," *IEEE Transactions on Energy Conversion*, vol. 38, no. 2, Jun. 2023.

Fazel Pourmirzaei Deylami was born in Astaneh Ashrafieh, Gilan, Iran, in 1993. He received his BSc degree in Electrical Engineering from the University of Guilan, Rasht, Iran, in 2015 and his MSc degree from Shahrood University of Technology, Shahrood, Iran, in 2019. He is now working toward his PhD degree in Electrical Engineering at Shahrood University of Technology, Shahrood, Iran. His research interests include design, modeling, and manufacturing of electrical machines.

Mahdi Akbari was born in Qom, Iran in 1995. He received his BSc degree in Mechanical Engineering from Amirkabir University of Technology, Tehran, Iran, in 2018, and his MSc degree in Mechatronics Engineering from Sharif University of Technology, Tehran, Iran, in 2020. His research interests include design and manufacturing of mechatronics systems.

Maedeh Emami was born in Theran, Iran in 1991. She received her BSc degree in Electrical Engineering from Islamic Azad University (Abhar Branch), Abhar, Iran, in 2014, and her MSc degree in Electrical Engineering from Islamic Azad University (Qazvin Branch), Qazvin, Iran, in 2018. Her research interests include software and hardware development of electronic systems.

Mohammad Amin Rezaei Gazik was born in Tehran, Iran, in 1998. He received his BSc degree in Electrical Engineering from the Ferdowsi University of Mashhad, Mashhad, Iran, in 2020, and his MSc degree in Electrical Engineering from Shahid Beheshti University, Tehran, Iran, in 2022. His research interest include power electronics and drive systems.

Ali Ashrafian was born in Karaj, Iran, in 1997. He received his BSc degree in Mechanical Engineering from Iran University of Science and Technology, Tehran, Iran, in 2020, and his MSc degree in Solid Mechanics from Sharif University of Technology, Tehran, Iran, in 2022, His research areas include finite element analysis and mathematical modeling.

Mohammad Javad Kamali was born in Shiraz, Iran in 1997. He received his BSc degree in Mechanical Engineering from Yazd University, Yazd, Iran, in 2020, and his MSc degree in Mechanical Engineering from Amirkabir University of Technology (Tehran Polytechnic), Tehran, Iran, in 2023. His research interests include design and manufacturing of robotic systems.